A COMPARISON OF TWO POROSITY-PERMEABILITY RELATIONS IN NUMERICAL SIMULATIONS OF SOLIDIFICATION OF METAL ALLOYS

M. Pilotelli, A.M. Lezzi, G.P. Beretta

Dipartimento di Ingegneria Meccanica, Università degli Studi di Brescia
via Branze 38, I-25123 Brescia, Italy

ABSTRACT

Solidification of an iron-carbon alloy is investigated through numerical simulations performed with a general-purpose CFD code. Only one set of conservation equations for binary solid-liquid phase change systems is solved throughout the entire domain, thus allowing the use of a fixed grid. The solidifying alloy is represented as a porous matrix (solid phase) at rest, filled with the liquid phase. Porosity, which is equal to 0 and 1 for fully solid and fully liquid material, respectively, is taken linearly dependent on temperature in the mush. Release of latent heat during phase change is accounted for by use of an effective specific heat, but solute transport is neglected. The effects of two different relations between porosity and permeability are compared by solving a case of solidification in a small rectangular cavity cooled from the sidewalls. It is found that for Rayleigh number up to 2.3×10^6 there is not appreciable influence of the permeability model on the overall heat transfer process, however, significant differences between the velocity fields near the liquidus line suggest important effects on solute transport.

1. INTRODUCTION

Solidification of metals as occurs in industrial ingot casting is a complex process affected by several phenomena. Appearance, properties, and quality of the ingot — the final product of the process — depend on many factors: mass, surface-to-volume ratio, and shape of the ingot; size and shape of the feedhead; material, mass, and wall thickness of the mold; forced convection effects during the mold-filling stage; natural convection effects during the ingot-solidification stage; use of insulating materials coupled to exothermic reactions at the ingot upper surface to delay solidification of the feedhead; presence of an insulating gap, partially filled with dust and gases, between the ingot and the mold etc.

Today's availability of general-purpose CFD packages with capabilities of modelling a large variety of physical phenomena in complex geometries, serves as a stimulus to attempt a heat transfer analysis of an industrial process in order to verify the extent to which numerical results are reliable and useful to the process engineer and the designer. With this spirit, we started numerical research work on ingot casting with the long-term goal of improving mold design for large-size steel ingots.

Phase transition between liquid and solid for metal alloys takes place over a finite temperature range. During ingot solidification this causes the formation of a two-phase region, referred to as the mushy region, which separates the solidus from the liquidus. In the liquid and in the mushy regions, temperature differences and constituent concentration differences may induce free convection flows. These motions have significant effects on the evolution of the mushy region itself, and are considered the cause of macrosegregation [1, 2].

Numerical methods to solve solidification problems can be classified into two classes. The first type subdivides the solution domain in regions (solid region, liquid region, etc.). Different conservation equations are solved in each region and the solutions are coupled by imposing proper conditions at the boundaries between regions. A deforming grid is necessary for each region. These methods are more suited for modelling solidification of a pure substance, since in this case a single moving boundary separates the liquid from the solid, rather than a mushy region of finite width.

In the second class of methods, only one set of conservation equations is solved throughout the entire domain. This allows the use of a fixed grid and avoids the difficulties associated with moving-boundary problems. The solidifying material is treated as a pseudo-porous medium (the solid phase) filled with a fluid (the liquid phase). The porosity of the medium varies both in time and in space, being equal to zero in the fully solid region, equal to unity in the fully liquid region and ranging between zero and unity in the mush.

Conservation equations for the pseudo-porous medium are obtained either through classical mixture theory [3, 4] or by use of volume averaging techniques. They can be cast in a form identical to the Navier-Stokes equations with the addition of source terms. This fact, together with the use of a single, fixed numerical grid makes numerical treatment of the solidification problem feasible with most general-purpose CFD codes.

The source term in the energy equation accounts for the gradual release of the latent heat of fusion in the mushy region. Upon introduction of an effective specific heat, the equation can be recast in a form that does not contain any source term.

The source term in the momentum equation models the momentum exchange between the two phases in the mushy

region. The models currently available are designed so that, in the mushy region, the momentum equation reduces to Darcy's law. In the fully liquid region, instead, the source term vanishes.

Darcy's law prescribes a linear relation between velocity and pressure gradient with a coefficient depending on the permeability of the porous medium. Different forms of the porosity-permeability relationship have been proposed in the literature for some solidifying materials. However, due to the paucity of data — especially for liquid fraction close to unity — there is no general agreement on any one of these forms.

In this paper we present the first results of a numerical study on steel ingot solidification. In particular, two different porosity-permeability relations are compared by solving a simple model of ingot solidification with the CFD code Fluent/UNS. The ingot is represented as a 2:1 aspect ratio rectangular cavity with prescribed heat flux at the sidewalls, and insulated upper and lower walls. In this preliminary work attention is focused on the effects of different permeability models on important aspects of the solidification process such as the rate of solid formation and the shape of the mushy region. For this reason and for the sake of simplicity, solute concentration is assumed uniform even if advective solute redistribution is known for being a critical issue in ingot casting [2].

2. MATHEMATICAL FORMULATION

In this work steel is treated rather simply as a binary alloy. Following the approach developed by Incropera and coworkers [3, 4], both phases of the solidifying material are viewed as continuum mixtures of iron and carbon coexisting in any region of space with varying volume fractions. Separate conservation equations of mass, momentum, energy, and species, are written for the liquid and the solid phase. These equations are summed up to obtain the following conservation equations for the alloy, which are valid in the mushy region as well as in the liquid and solid regions,

$$\frac{\partial \rho}{\partial t} + \nabla \cdot (\rho \mathbf{u}) = 0 \tag{1}$$

$$\frac{\partial}{\partial t}(\rho u_i) + \nabla \cdot (\rho \mathbf{u} u_i) = \nabla \cdot \left(\sum_k g_k \, (\mathbf{e}_{(i)} \cdot \boldsymbol{\sigma}_k) \right) + \rho B_i + \\ -\nabla \cdot \left(\sum_k \bar{\rho}_k \, (\mathbf{u}_k - \mathbf{u}) \, (u_{k\,i} - u_i) \right) \quad \text{for } i = 1,\, 2,\, 3 \tag{2}$$

$$\frac{\partial}{\partial t}(\rho H) + \nabla \cdot (\rho \mathbf{u} H) = \nabla \cdot \left(\sum_k g_k \, k_k \, \nabla T \right) + \\ -\nabla \cdot \left(\sum_k \bar{\rho}_k \, (\mathbf{u}_k - \mathbf{u}) \, (H_k - H) \right) \tag{3}$$

$$\frac{\partial}{\partial t}(\rho \, f^\alpha) + \nabla \cdot (\rho \mathbf{u} \, f^\alpha) = \nabla \cdot \left(\sum_k \bar{\rho}_k D_k^\alpha \nabla f_k^\alpha \right) + \\ -\nabla \cdot \left(\sum_k \bar{\rho}_k \, (\mathbf{u}_k - \mathbf{u}) \, (f_k^\alpha - f^\alpha) \right). \tag{4}$$

Equations (1)–(4) contain quantities relative to a single phase — denoted by subscript k — such as, for example, g_k and $\mathbf{u}_k$ which are the volume fraction and the velocity of phase k, and quantities relative to the alloy such as ρ and $\mathbf{u}$.

Alloy properties are defined as either mass or volume averages of phase variables. If ρ_k is the actual density of phase k, upon introduction of the phase partial density

$$\bar{\rho}_k = g_k \, \rho_k \tag{5}$$

the alloy density is defined as

$$\rho = \sum_k \bar{\rho}_k. \tag{6}$$

The mass fraction of phase k is

$$f_k = \frac{\bar{\rho}_k}{\rho}. \tag{7}$$

The alloy velocity is the mass average of the velocities of the individual phases

$$\mathbf{u} = \frac{1}{\rho} \sum_k \bar{\rho}_k \, \mathbf{u}_k = \sum_k f_k \, \mathbf{u}_k. \tag{8}$$

Similarly, the alloy body force, enthalpy, and concentration of species α are defined as

$$\mathbf{B} = \sum_k f_k \, \mathbf{B}_k \qquad H = \sum_k f_k \, H_k \qquad f^\alpha = \sum_k f_k \, f_k^\alpha \tag{9}$$

where in the last expression f_k^α is the mass fraction of species α in phase k.

The thermal conductivity of the alloy is defined as the volume average of the corresponding properties of individual phases

$$k = \sum_k g_k \, k_k. \tag{10}$$

Equation (3) is based on the assumption — referred to in the following as assumption (A.1) — of local thermodynamic equilibrium among the phases, so that $T_k = T$ for all k. In addition, in Eqs. (2)–(4) the advective term is decomposed into the contribution due to the mean alloy motion, on the left hand side of the equations, and the contributions due to the relative phase motion which is the last term on the right hand side.

For a two-phase solid-liquid system, such as solidifying steel, upon making some simplifying hypothesis, Eqs. (2) and (3) reduce to a form which is amenable of solution with most general-purpose CFD codes. Following Refs.[1, 2, 4, 5], here we take the following assumptions.

(A.2) The solid phase behaves like a rigid body at rest,

$$\mathbf{u}_s = 0 \tag{11}$$

(A.3) The liquid phase behaves as a Newtonian fluid.

(A.4) Density, viscosity, thermal conductivity, and specific heat are uniform and constant for each phase.

(A.5) Buoyancy effects due to density variations are accounted for using the Boussinesq approximation.

(A.6) Density and specific heat are equal for the phases, i.e.,

$$\rho_{\rm s} = \rho_{\rm l} = \rho \tag{12}$$

$$c_{\rm s} = c_{\rm l} = c. \tag{13}$$

Therefore,

$$g_k = f_k \quad \text{for } k = {\rm s}, {\rm l}. \tag{14}$$

(A.7) Gravity is the only body force.

(A.8) Solute concentration f^α is uniform and constant.

As a consequence of assumptions (A.2) and (A.6) the continuity equation reduces to

$$\nabla \cdot (f_{\rm l} \mathbf{u}_{\rm l}) = 0. \tag{15}$$

For a uniform and constant solute concentration, Eq. (4) is automatically satisfied. In addition, the closure of the system of conservation equations requires a relation between liquid fraction and temperature in the mushy region which we take linear — assumption (A.9) — as in Ref. [5],

$$f_{\rm l} = g_{\rm l} = \frac{T - T_{\rm sol}}{T_{\rm liq} - T_{\rm sol}} \tag{16}$$

where $T_{\rm liq}$ and $T_{\rm sol}$ are the liquidus and the solidus temperatures of the binary alloy for the prescribed solute concentration.

2.1 Momentum equation

Equation (2) contains the individual phase stress tensors $\boldsymbol{\sigma}_k$. Under conditions (A.1), (A.3) and (A.4) the liquid phase stress term takes the following form

$$\nabla \cdot \left(g_{\rm l} \left(\mathbf{e}_{(i)} \cdot \boldsymbol{\sigma}_{\rm l} \right) \right) = \mu_{\rm l} \nabla \cdot \left(\frac{\rho}{\rho_{\rm l}} \nabla u_i \right) - \frac{\partial}{\partial x_i} \left(g_{\rm l}\, p \right). \tag{17}$$

Because of the assumption (A.2) of rigid body behavior, particular care is required in developing the solid phase stress term. As proposed in Ref. [4], starting from the solid phase momentum equation,

$$\nabla \cdot \left(g_{\rm s} \left(\mathbf{e}_{(i)} \cdot \boldsymbol{\sigma}_{\rm s} \right) \right) = -\bar{\rho}_{\rm s} B_{{\rm s}\,i} - g_{\rm s} \dot{G}_{{\rm s}\,i} \tag{18}$$

where $g_{\rm s}\dot{G}_{{\rm s}\,i} = -g_{\rm l}\dot{G}_{{\rm l}\,i}$ represents the momentum exchange from liquid to solid due to pressure, viscous shear, and phase change, separating normal from shear forces, neglecting momentum exchange due to phase change, one obtains

$$\nabla \cdot \left(\sum_k g_k \left(\mathbf{e}_{(i)} \cdot \boldsymbol{\sigma}_k \right) \right) + \rho B_i = \mu_{\rm l} \nabla \cdot \left(\frac{\rho}{\rho_{\rm l}} \nabla u_i \right) - g_{\rm l} \left(\frac{\partial p}{\partial x_i} - \rho_{\rm l} B_{{\rm l}\,i} - \dot{G}_{D\,{\rm l}\,i} \right) \tag{19}$$

where $\dot{G}_{D\,{\rm l}\,i}$ is the drag exerted by the solid phase on the liquid phase. In order to close the system of equations it is necessary to find an explicit expression for the drag interaction term. In metallurgical studies [5] (see also [2, 4, 6]) it is common to consider the dendritic structure that forms and grows during solidification as a porous matrix filled with liquid metal, and to assume — assumption (A.10) — that Darcy's law is applicable to describe flow in the mush

$$\nabla p - \rho_{\rm l} \mathbf{B}_{\rm l} = -\frac{\mu_{\rm l}}{K} g_{\rm l} \mathbf{u}_{\rm l}. \tag{20}$$

In Eq. (20) K is the permeability of the porous medium which is assumed isotropic — assumption (A.11). According to assumption (A.10), in the mushy region the dominant terms of the momentum equation reduce to Darcy's law, therefore comparison of Eqs. (2) and (19) with Eq. (20) shows that the drag term can be written as

$$\dot{G}_{D\,{\rm l}\,i} = -\frac{\mu_{\rm l}}{K} u_i. \tag{21}$$

Substituting Eq. (21) in (19) and recalling assumption (A.6), the momentum equation takes the following form

$$\frac{\partial}{\partial t} (\rho \mathbf{u}) + \nabla \cdot (\rho \mathbf{u}\mathbf{u}) = \mu_{\rm l} \nabla^2 \mathbf{u} + - \left(\nabla p - \rho \mathbf{B}_{\rm l} + \frac{\mu_{\rm l}}{K} \mathbf{u} \right) - \nabla \cdot \left(\rho \frac{f_{\rm s}}{f_{\rm l}} \mathbf{u}\mathbf{u} \right). \tag{22}$$

In Eq. (22) the term $g_{\rm s} \left(\nabla p - \rho \mathbf{B}_{\rm l} + \mu_{\rm l} \mathbf{u}/K \right)$ has been neglected because it is identically zero in the liquid and vanishingly small in the mush where Darcy's law applies.

Some authors [2, 5] do not even mention the advective term due to relative phase motion — the last term on the right hand side of Eqs. (2) and (22) — which is indeed negligible. Actually, this term is different from zero only in the mush where, according to the scaling analysis of Krane and Incropera [7], its order of magnitude is equal to that of the mean motion advective term times $f_{\rm s}/f_{\rm l}$. Therefore, where convective effects are more important, i.e. for $f_{\rm s} \ll 1$, this term is much smaller than the mean motion advective term. Instead, for $f_{\rm s} \sim 1$ both advective terms are negligible compared to the interphase drag term. Thus, a non significant error is introduced upon neglecting this term everywhere in the alloy.

Finally, the momentum equation can be recast in the following form

$$\frac{\partial}{\partial t} (\rho \mathbf{u}) + \nabla \cdot (\rho \mathbf{u}\mathbf{u}) = -\nabla p' + \mu_{\rm l} \nabla^2 \mathbf{u} - \rho \beta \left(T - T_0 \right) \mathbf{g} + \mathbf{S}_{\rm m} \tag{23}$$

where the Darcian damping term is represented as a momentum source

$$\mathbf{S}_{\rm m} = -\frac{\mu_{\rm l}}{K} \mathbf{u}. \tag{24}$$

In writing Eq. (23), use is made of assumptions (A.7) and (A.5). Thus p' represents the pressure without the hydrostatic contribution and T_0 is a reference temperature.

2.2 Porosity-permeability relations

The coefficient K which appears in Darcy's law depends on the size and shape of interstices of the solid matrix. For a given shape it is roughly proportional to the square of their linear dimension. Therefore, for a non homogeneous porous medium such as the mush, permeability is expected to vary in space and time as a consequence of liquid fraction variations.

Several expressions of K — based on different conceptual models of the porous medium — are available in literature [8, chap. 5].

In the simplest approach the porous matrix is modelled as a bundle of capillary pipes in each of which the flow is of Poiseuille type. The resulting form of K is

$$K = c_0 \frac{\lambda^3}{(1-\lambda)^2} \frac{1}{M_s^2}. \tag{25}$$

Equation (25) is known as Kozeny-Carman equation. Kozeny's constant c_0 depends on channel shape and is determined by fitting experimental data. The porosity λ of the mushy region of a solidifying alloy is usually considered equal to the liquid volume fraction. M_s represents the ratio of wetted solid surface to solid volume.

Most numerical studies on solidification of binary systems use Eq. (25) setting the ratio $C = c_0/M_s^2$ equal to a constant [1, 5, 7]. The value of the constant depends on the average dendritic arm spacing: in Ref. [1], for example, C is taken equal to 1.4×10^{-9} and 2.8×10^{-11} m^2 for Al-14.9wt%Mg and Pb-19.2wt%Sn, respectively. However, assuming M_s constant, does not seem appropriate. In a bundle of tubes, M_s decreases as their average distance increases, therefore, one expects at least a weak dependence of M_s on porosity. As a matter of fact experiments performed by Piwonka and Flemings show that K is proportional to λ^2 rather than to λ^3 for λ smaller than approximately 1/3 [9].

This behavior is predicted by the so-called resistance-to-flow models. In this approach, the porous medium is represented as a densely packed, regular or random array of small bodies. From a knowledge of the drag exerted by a creeping flow on a single particle, it is possible to obtain expressions for the permeability. For example, permeability for an assemblage of roughly spherical particles can be written as

$$K = c_1 \frac{\lambda^2}{1-\lambda} d^2 \tag{26}$$

where d is the diameter of the particles and c_1 is a constant that depends on the particles shape and their average distance.

In a numerical computation of solute redistribution in an iron-carbon alloy, Amberg [2] uses a porosity-permeability relation due to West [6] that reduces to Eq. (26) for small values of λ. The relation proposed by West is based on the experimental evidence of two distinct trends in permeability behavior of metal mush [6, 9]. At low values of liquid fraction ($g_\mathrm{l} < 0.3$) permeability increases as λ^2, but at larger values of g_l, it increases much more rapidly. The mushy zone, therefore, cannot be described through a single model, but at least two models are necessary to describe the transition from interstices in a solid body (low liquid fraction) to particles in a liquid (low solid fraction).

The relation proposed by West is the following,

$$K = C_1\,\lambda^2 + C_2\,\mathrm{H}\left(\lambda - \frac{1}{3}\right) \times (1-\lambda)^{2/3}\left(\frac{7-3\lambda}{1-\lambda} - 3\sqrt{\frac{5+3\lambda}{1-\lambda}}\right) \tag{27}$$

where $\mathrm{H}(\lambda - 1/3)$ is the Heaviside function which vanishes for $\lambda < 1/3$ and is identically 1 for $\lambda > 1/3$. The first term on the right hand side of Eq. (27) is similar to Eq. (26) and represents permeability of a compact assemblage of small particles, the second term gives the permeability of an array of separated spheres. C_1 and C_2 are empirically determined constants.

In this work we investigate the effects of different permeability expressions on numerical computation of steel solidification. The equations to be compared are the West equation (27) and the Kozeny-Carman equation (25).

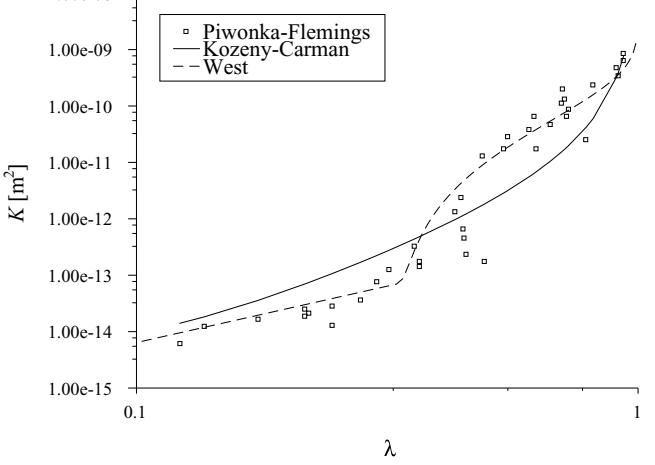

Figure 1: Permeability *vs* porosity: Kozeny-Carman equation (solid line) and West equation (dashed line). Squares represent experimental data in Ref. [9].

Following Amberg, who studies a mixture of iron and carbon, we take for constants C_1 and C_2 in Eq. (27) the values 6.4×10^{-13} and 8.8×10^{-11} m^2, respectively. They have been determined by using the experimental data in Ref. [9], even if data refer to a Al-4.5wt%Cu alloy.

For consistency, we have estimated the ratio $C = c_0/M_s^2$ that appears in the Kozeny-Carman equation, by best fitting the data in Ref. [9] to Eq. (25). The value obtained in this way is $C = 3.84 \times 10^{-12}$ m^2. Both porosity-permeability relations are plotted in Fig. 1, together with the experimental data of Piwonka and Flemings.

2.3 Energy equation

As for the momentum equation, also for the energy equation the advective term due to relative phase motion — last term on the right hand side of Eq. (3) — can be neglected. Indeed, the order of magnitude of this term is equal to that of the advective term due to mean motion times f_s. Therefore, for $f_\mathrm{s} \to 0$, where convective effects are dominant, it is smaller than the mean motion advective term.

Most general-purpose CFD codes solve the energy equation using temperature as an independent variable, thus it is necessary to express the alloy enthalpy as a function of T. If phase enthalpy is written as

$$H_k = H_{k\,\mathrm{ref}} + \int_{T_\mathrm{ref}}^{T} c_k\,dT \tag{28}$$

and assumptions (A.4) and (A.6) are adopted, the alloy total enthalpy can be written as

$$H = H_{\mathrm{s\,ref}} + \int_{T_\mathrm{ref}}^{T} c\,dT + g_\mathrm{l} L \tag{29}$$

where $L = H_{\mathrm{l\,ref}} - H_{\mathrm{s\,ref}}$ is the heat of fusion which is gradually released during solidification.

By separating the sensible heat

$$h = H_{\mathrm{s\,ref}} + \int_{T_\mathrm{ref}}^{T} c\,dT \tag{30}$$

from the latent heat

$$\Delta H = \frac{T - T_{\rm sol}}{T_{\rm liq} - T_{\rm sol}} L \tag{31}$$

where use is made of the lever rule (16), the energy equation becomes

$$\frac{\partial}{\partial t}(\rho h) + \nabla \cdot (\rho \mathbf{u} h) = \nabla \cdot (k \nabla T) + S_e \tag{32}$$

where the source term on the right hand side

$$S_e = -\left[\frac{\partial}{\partial t}(\rho \Delta H) + \nabla \cdot (\rho \mathbf{u} \Delta H)\right]. \tag{33}$$

This approach is that used in Refs. [2] and [5].

An alternative approach is the introduction of an effective specific heat which takes into account the latent heat,

$$c_e = c + \mathrm{H}(T - T_{\rm sol})\,\mathrm{H}(T_{\rm liq} - T)\,\frac{L}{T_{\rm liq} - T_{\rm sol}} \tag{34}$$

which is equal to $c + L/(T_{\rm liq} - T_{\rm sol})$ for T between the solidus and the liquidus temperature, and coincides with c otherwise. In this case the energy equation is simply

$$\frac{\partial}{\partial t}(\rho H) + \nabla \cdot (\rho \mathbf{u} H) = \nabla \cdot (k \nabla T) \tag{35}$$

with the total enthalpy calculated as

$$H = H_{\rm s\,ref} + \int_{T_{\rm ref}}^{T} c_e \, dT. \tag{36}$$

This form is that used for this work.

3. NUMERICAL RESULTS

To compare the effect of different porosity-permeability relations on the numerical computation of a solidification process, the same two-dimensional problem addressed by Amberg in Ref. [2] has been chosen.

The configuration of the test problem is shown in Fig. 2. A Fe-1wt%C alloy solidifies in a small rectangular cavity of height $l = 0.1$ m and width $2l$. The upper and lower walls are thermally insulated, whereas a uniform and constant heat flux $\dot{q} = 60$ kW/m^2 is removed from the sidewalls, starting at time $t = 0$.

Initially the melt in the cavity is at rest, at uniform temperature $T_{\rm i} = 1736$ K, 5 K above the liquidus temperature. The problem exhibits symmetry about the vertical midplane. Therefore, upon introduction of a frame of reference centered at the bottom left corner with horizontal coordinate x and vertical coordinate y, numerical computations are restricted to the square $0 < x < l$, $0 < y < l$.

The values of the thermophysical properties of the iron-carbon alloy used for calculations are taken from Ref. [2] and are summarized in Tab. 1. In particular, the liquidus and solidus temperatures, calculated for a constant carbon mass fraction of 1%, are 1731 and 1623 K, respectively. The reference temperature in the Boussinesq term is set equal to the fusion temperature of pure iron, $T_0 = 1809$ K.

The code used for numerical computations is Fluent/UNS v. 4.1. Based on a finite volume

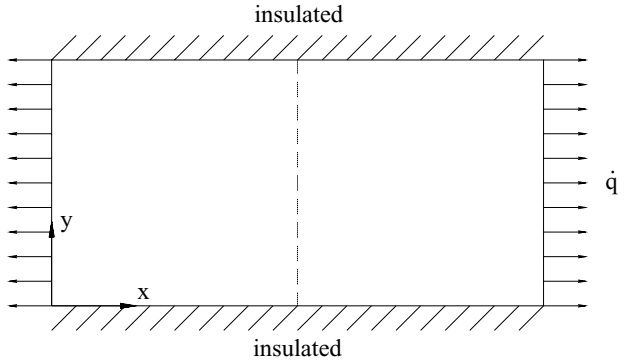

Figure 2: Test problem geometry.

discretization technique, Fluent/UNS solves mass, momentum and energy equations in a rather general form which contains Eqs. (1), (23), and (35).

The finite volume approach requires that source terms be linearized. If ϕ is the variable that is being solved for, the source term has to be written as $S = a + b\phi$, where a and b may themselves depend on ϕ. To avoid divergence of the numerical solution, it is important that b be a non-positive quantity [10, Chap. 3]. The source term which appears in Eq. (23) is already a linear function of the alloy velocity with the constant term a identically zero and negative linear coefficient $b = -\mu_{\rm l}/K$. It can be easily included into the code by writing a user-defined function in C language which is compiled and linked at runtime from within the code itself.

If permeability is expressed using either the West equation or the Kozeny-Carman equation, the linear coefficient b diverges as porosity tends to zero. Thus permeability expressions are modified to avoid occurrence of numerical overflow. We set

$$b_{\rm I} = -\mu_{\rm l}\left[C_1\,(\lambda + \varepsilon_{\rm I})^2\right]^{-1} \qquad \text{for } 0 \le \lambda \le \frac{1}{3} \tag{37}$$

$$b_{\rm I} = -\mu_{\rm l}\left[C_1\,\lambda^2 + C_2\,(1-\lambda)^{2/3}\left(\frac{7-3\lambda}{1-\lambda} + -3\sqrt{\frac{5+3\lambda}{1-\lambda}}\right)\right]^{-1} \qquad \text{for } \frac{1}{3} < \lambda \le 1 \tag{38}$$

and, following the example of Voller and Prakash [5],

$$b_{\rm II} = -\mu_{\rm l}\frac{(1-\lambda)^2}{C\,(\lambda^3 + \varepsilon_{\rm II})} \tag{39}$$

where $\varepsilon_{\rm I} = 0.01$ and $\varepsilon_{\rm II} = 0.001$.

About the energy equation, since Fluent/UNS allows to define the specific heat as a stepwise function of temperature, the effective specific heat approach has been preferred for its semplicity. The alloy thermal conductivity is calculated through a user-defined function using Eq. (10).

Computations have been performed on a 152 × 38 orthogonal grid with uniform spacing in both x and y direction. The number of cells in the x direction is quadrupled with respect to the 38 × 38 grid used by Amberg [2]. This is necessary to avoid divergence of the numerical solutions in the early stage of solidification. During calculations both *PRESTO!* and

Table 1: Data for test problem

Cavity height and half width	$l = 0.1$ m
Wall heat flux	$\dot{q} = 60$ kW m^{-2}
Initial temperature	$T_{\rm i} = 1736$ K
Density	$\rho = 6940$ kg m^{-3}
Specific heat	$c = 753$ J kg^{-1} K^{-1}
Dynamic viscosity	$\mu = 6.94 \times 10^{-3}$ kg m^{-1} s^{-1}
Liquid thermal conductivity	$k_{\rm l} = 30$ W m^{-1} K^{-1}
Solid thermal conductivity	$k_{\rm s} = 60$ W m^{-1} K^{-1}
Liquidus temperature	$T_{\rm liq} = 1731$ K
Solidus temperature	$T_{\rm sol} = 1623$ K
Solid reference enthalpy	$H_{\rm s\,ref} = 0$ J kg^{-1}
Reference temperature	$T_{\rm ref} = 298.15$ K
Enthalpy of fusion	$L = 2.72 \times 10^5$ J kg^{-1}
Thermal coefficient of expansion	$\beta = 2.71 \times 10^{-4}$ K^{-1}
Reference temperature	$T_0 = 1809$ K

Implicit Body Force Treatment options have been enabled, as recommended for natural convection applications [11, Chap. 12]. First-order upwind discretization scheme for the advective terms has been used throughout all computations. The fixed number of iterations performed for each time step has been chosen sufficiently large so that residuals level out. Calculations have been performed on a PC equipped with two Intel Pentium 133 processors.

Several preliminary tests were performed. First, we tried and reproduced with very good agreement the results obtained by Voller and Prakash in Ref. [5]. It is noteworthy that the agreement is very good even though the release of heat of fusion is represented through the source term described by Eq. (33) in the work by Voller and Prakash, whereas we use the equivalent specific heat method. Next, we tried to solve the test problem described above, using the momentum source term $b_{\rm I}\mathbf{u}$ based on the West equation, but the code failed to reach convergence shortly after the appearence of the mushy region. Many trial calculations were necessary to adjust the time step, the values of the underrelaxation factors, and the cell size in the x direction to make the solver converge throughout the entire solidification process.

Three simulations of the solidification process have been carried out. In the first simulation we use the modified West equation (37-38). During this simulation it has been difficult to attain convergence. The time step has been set to 0.1 s for the initial stage, then modified to 0.2 s and, after the liquid region disappeared, progressively increased up to 5 s. The underrelaxation factors have been kept equal to 0.1, which is a value much smaller than the default ones. As a consequence, the number of iterations allowed for each time step has been increased to 150. Computations required about 303 h for 3600 s of simulated time. Despite the small values of the underrelaxation factors, residuals exhibited an oscillating behavior during several time steps. This anomalous behavior is observed only when both the liquid and the mushy regions are present. We identify the cause of difficulties in convergence in the very rapid change of the West equation as porosity tends to 1 (see Fig. 3).

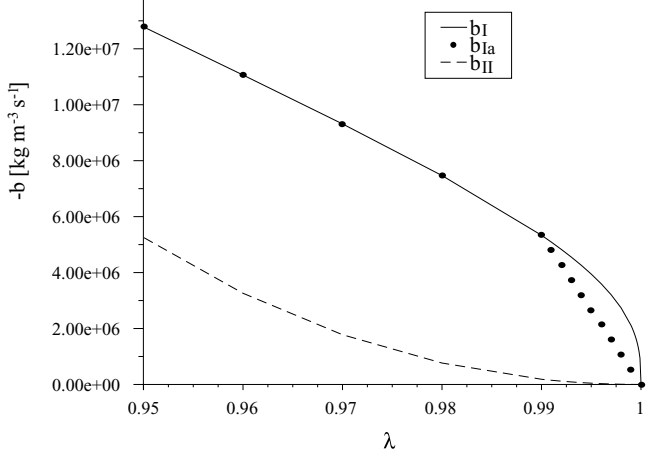

Figure 3: Momentum source linear coefficients used in numerical simulations: asymptotic behavior as porosity tends to 1.

Indeed Eq. (38) is asymptotic to $-(\mu_{\rm l}/4C_2)(1-\lambda)^{1/3}$ as $\lambda \to 1$ and has infinite slope at $\lambda = 1$. To avoid this singularity we have further modified the momentum source linear coefficient, imposing a linear behavior for $0.99 \le \lambda \le 1$, as shown in Fig. 3,

$$b_{\rm Ia} = b_{\rm I} \quad \text{for } 0 \le \lambda \le 0.99 \tag{40}$$

$$b_{\rm Ia} = b_{\rm I}(\lambda)|_{\lambda=0.99}\,\frac{1-\lambda}{0.01} \quad \text{for } 0.99 \le \lambda \le 1. \tag{41}$$

The second simulation has been performed using $b_{\rm Ia}\mathbf{u}$ as momentum source term. The beneficial effects of the modification of b are: to allow larger time steps — 0.2 s at the beginning, 1 s until disappearance of the liquid region, and 5 s later on — and higher underrelaxation factors, set to 0.5; to reduce to 50 the number of iterations per time step; and to eliminate oscillations of residuals. As a consequence of these changes the computation time required for 3600 s of simulated time decreased to 87 h. This second simulation ended at $t = 4370$ s upon complete solidification of the alloy. No significant differences can be observed between numerical results obtained using either $b_{\rm I}$ or $b_{\rm Ia}$, therefore in the discussion below we refer to the results of the second simulation only.

During the third simulation, the source term $b_{\rm II}\mathbf{u}$ based on the Kozeny-Carman equation, has been tested. As clearly shown in Fig. 3, $b_{\rm II}$ tends to zero with zero slope as λ approaches 1. This behavior seems to make convergence of the solver much easier. Indeed, for this simulation it was not necessary to change Fluent's default values of the underrelaxation factors. Moreover, larger time steps could be used — from 0.5 s at the beginning, up to 10 s when the liquid region was still present. Although as many as 100 iterations per time step were allowed during part of the simulation, the computation time for the first 3600 s amounted to about 36 h. Also in this case, the computation was stopped at $t = 4360$ s upon complete solidification.

Figs. 4-6 show isotherms — which coincide with isoporosity lines inside the mushy region — and velocity vectors at $t = 200$, 400, 3600 s for the second (West) and the third (Kozeny-Carman) simulations. At $t = 200$ s roughly half of the cavity is occupied by the mush. It

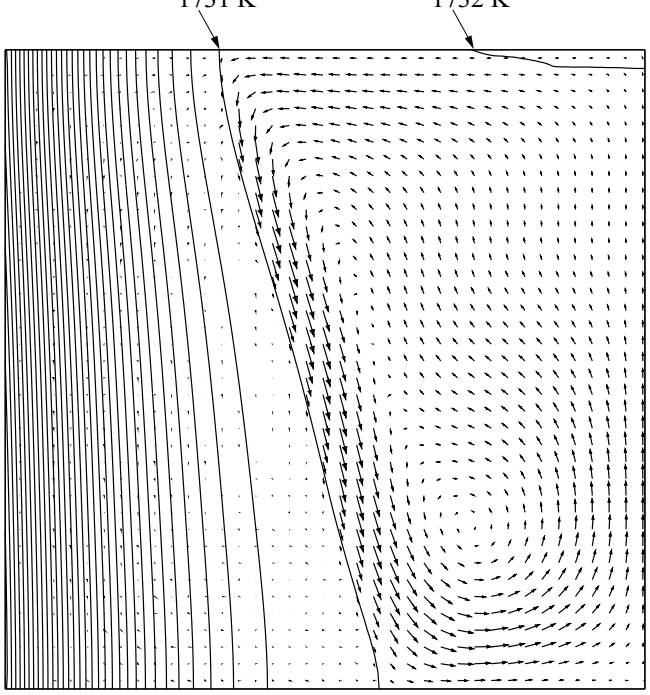

(a)

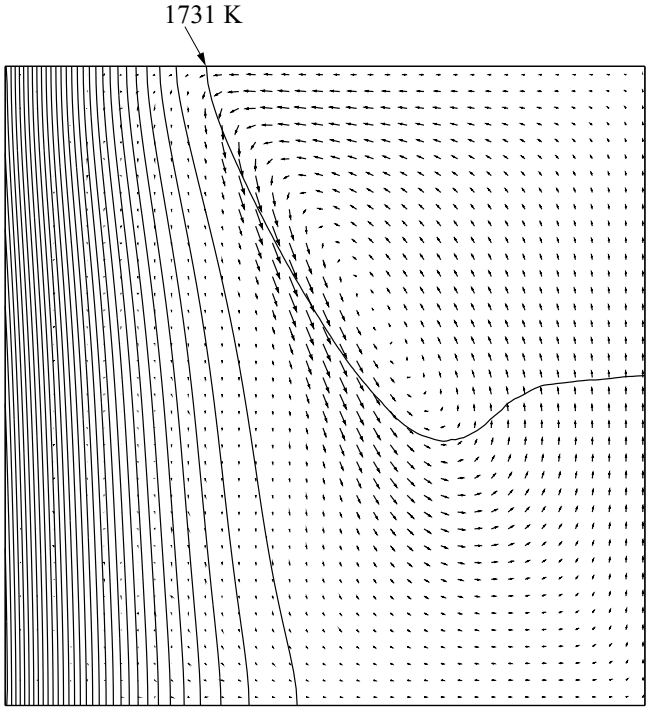

(b)

Figure 4: Isotherms and velocity vectors at $t = 200$ s: (a) West equation; (b) Kozeny-Carman equation. Isotherms are plotted in increments of 1 K. Liquidus temperature is 1731 K. In (a) $|\mathbf{u}|_{\max} = 4.16 \times 10^{-3}$ m/s, in (b) $|\mathbf{u}|_{\max} = 3.13 \times 10^{-3}$ m/s.

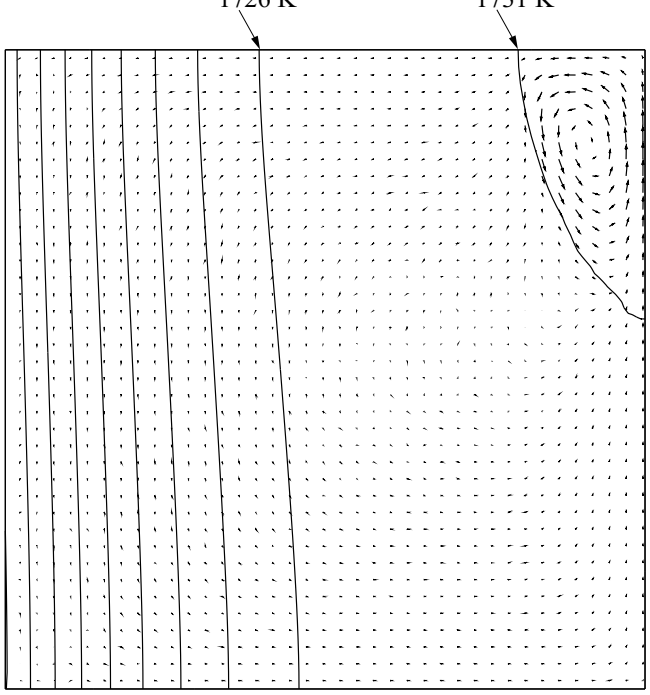

(a)

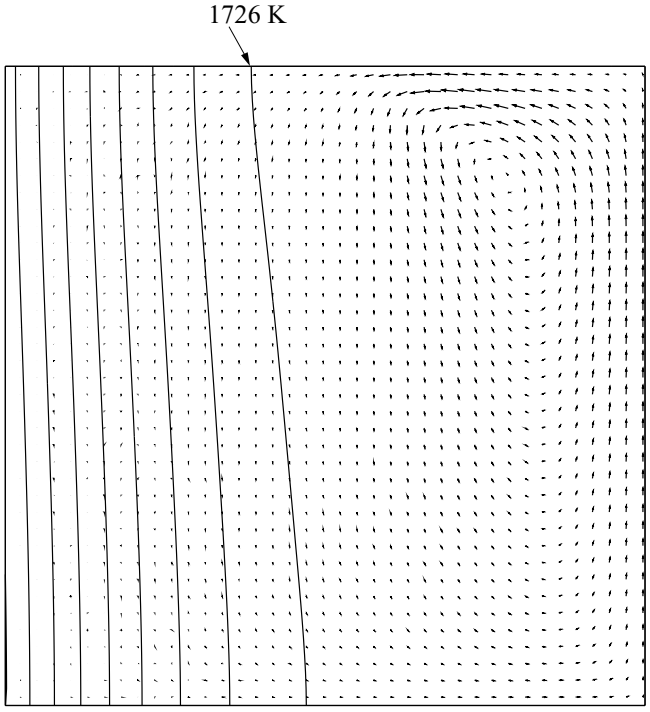

(b)

Figure 5: Isotherms and velocity vectors at $t = 400$ s: (a) West equation; (b) Kozeny-Carman equation. Isotherms are plotted in increments of 5 K. Liquidus temperature is 1731 K. Velocity vector scale is 5 times smaller than in Fig. 4.

is apparent an anticlockwise circulation induced by a jet of cooled liquid flowing downward, close to the liquidus line (1731 K). Maximum velocity is about 5×10^{-3} m/s. If advection were absent, isotherms would be vertical; the development of the slow recirculating motion due to natural convection, instead, keeps the liquid region almost isothermal, with a weak temperature gradient directed upward. The effect of advection extends to isotherms inside the mushy region which are inclined. The liquid region disappears at $t = 400$ s approximately. At this stage thermal convection is still appreciable in the more porous regions of the mush, even if velocities are

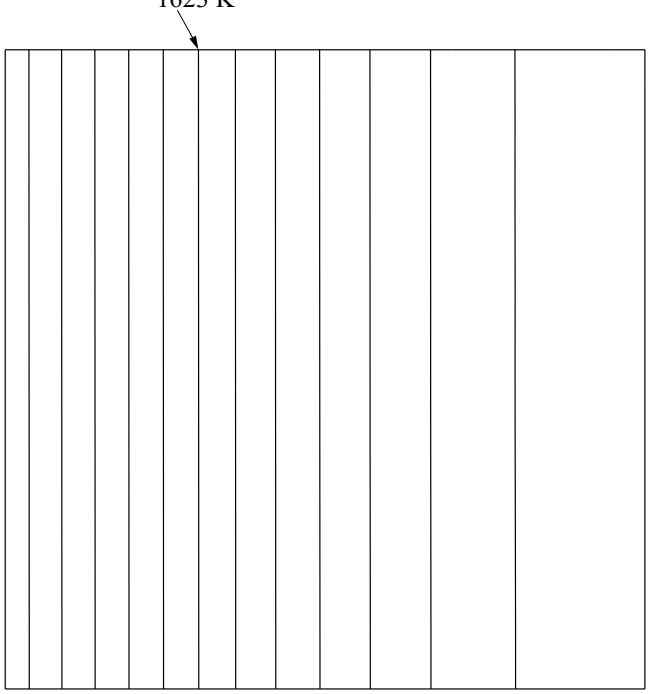

(a)

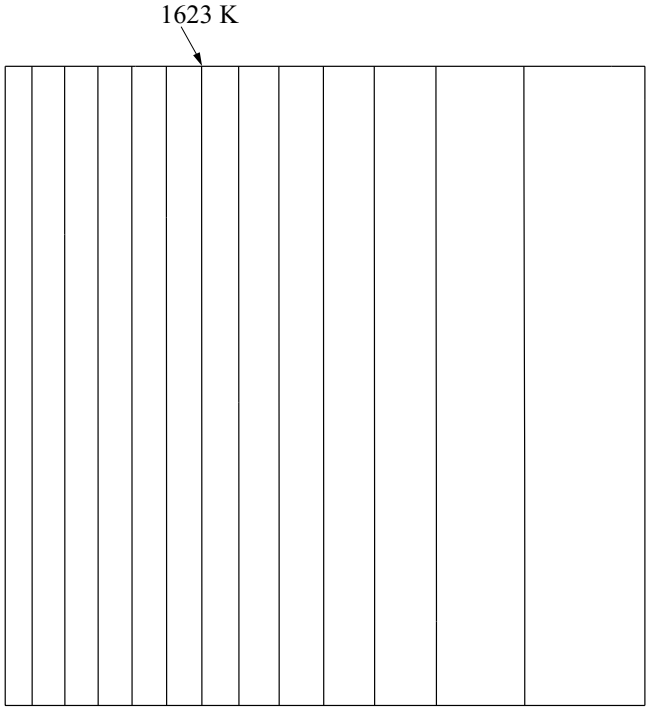

(b)

Figure 6: Isotherms and velocity vectors at $t = 3600$ s: (a) West equation; (b) Kozeny-Carman equation. Isotherms are plotted in increments of 5 K. Solidus temperature is 1623 K.

reduced by one order of magnitude. As cooling proceeds, permeability of the mush decreases rapidly and velocities become vanishingly small. Although thermal diffusion is now the only active mechanism of heat transfer, isotherms near the centerline are still inclined because the vertical temperature gradient established at the beginning of the process is not smoothed out yet. The fully solid region begins to form around $t = 2600$ s, when temperature distribution is practically one-dimensional. Later on, at $t = 4360$ s, the mushy region disappears and the alloy becomes completely solid.

How can we compare the effects of the two permeability expressions on ingot solidification? Global parameters such as the rate of solid formation coincide within 1% throughout the entire process, denoting a negligible influence of the form of the momentum source term. However, this indicator seems to deceive the key phenomena governing this test problem. Indeed, calculations performed assuming both phases at rest give the same rate of solid formation as in the cases where advection is present. The Rayleigh number based on the difference between initial and liquidus temperatures and on the cavity height l, is equal to 2.3×10^6. Although this value is sufficiently large, advection seems to act as a perturbation effect on the dominant diffusion transport, perhaps because of the type of boundary condition imposed on the sidewalls. Further tests are necessary to verify whether for higher Ra or smaller heat fluxes, the effect of the permeability expression on the heat transport process becomes appreciable. For the time being, we can only say that the choice of one of the two source terms investigated affects only the velocity fields and the isotherm patterns in the first phase of the solidification process.

It is apparent that the main differences between Figs. 4(a) and 5(a) (West) and Figs. 4(b) and 5(b) (Kozeny-Carman) are due to the different order of magnitude of b_{Ia} and b_{II} for porosity close to one, which produces dissimilar velocity fields in the mushy region close to the liquidus line. While the West equation induces an abrupt reduction of velocity across the boundary between liquid and mushy regions, the Kozeny-Carman equation is characterized by a smooth damping of velocity which allows significant flow rates inside the mush. These differences affect heat transfer appreciably only in the shape and relative position of isotherms between 1726 and 1731 K approximately. However, if transport of solute were taken into account, the numerically predicted solute distribution in the solidified ingot might be significantly affected by the permeability expression adopted. It has been observed [1, 2] that when solute concentration is allowed to vary, a clockwise circulation develops in the mush. This motion is due to solutal driven convection which overwhelms the thermally driven one and is the main cause of the enrichment of solute at the top of the ingot. Therefore, stronger flow rates in the mush, as those allowed by the Kozeny-Carman equation, might produce a more severe macrosegregation.

4. CONCLUSIONS

Solidification of an iron-carbon alloy has been investigated through numerical simulations performed with a general-purpose CFD code. In order to use a fixed grid, the solidifying alloy is represented as a porous matrix with temperature-dependent porosity (solid phase), at rest, filled with liquid (liquid phase). Release of heat of fusion during phase change is accounted for by introduction of an effective specific heat, but solute transport is neglected. Two relations between porosity and permeability are used in previous studies of binary alloys solidification. In this paper interest lies mainly in

comparing the effects of the choice between these relations.

We chose as test problem the same problem solved in Ref. [2] — solidification in a small rectangular 2D cavity cooled from the sidewalls. Difficulties in attaining numerical convergence for one of the permeability expressions is overcome through a small modification for porosity close to one. This change reduces computation time by a factor three without introducing significant differences.

Numerical results do not show appreciable influence of the permeability relations on the overall heat transfer process, however, there are clear differences between the velocity fields near the boundary between the mush and the liquid alloy. Since liquid motion through the mush is strictly related to solute segregation, this fact suggests that the permeability model adopted should affect quite importantly the transport of solute. The results presented are preliminary in that they have to be confirmed by further tests for different values of the Rayleigh number and different boundary conditions. In addition, differences between the two permeability expressions can be fully appreciated only if the transport equation for the solute (4) is included in the model.

NOMENCLATURE

a, b	coefficients in the linearized form of the source term
B, $\mathbf{B}$	body force per unit mass [$\mathrm{m\,s^{-2}}$]
c	specific heat [$\mathrm{J\,kg^{-1}\,K^{-1}}$]
c_e	effective specific heat [$\mathrm{J\,kg^{-1}\,K^{-1}}$]
c_0	Kozeny's constant [dimensionless]
C, C_1, C_2	constants in permeability expressions [$\mathrm{m^2}$]
D	mass diffusion coefficient [$\mathrm{m^2\,s^{-1}}$]
$\mathbf{e}_{(i)}$	i-th unit vector of a Cartesian right handed bases
f	mass fraction [dimensionless]
g	volume fraction [dimensionless]
$\mathbf{g}$	gravity acceleration [$\mathrm{m\,s^{-2}}$]
$\dot{G}$	momentum source due to phase interactions [$\mathrm{kg\,m^{-2}\,s^{-2}}$]
$\dot{G}_D$	momentum source due to shear forces between phases [$\mathrm{kg\,m^{-2}\,s^{-2}}$]
h	sensible heat [$\mathrm{J\,kg^{-1}}$]
ΔH	latent heat [$\mathrm{J\,kg^{-1}}$]
H	specific enthalpy [$\mathrm{J\,kg^{-1}}$]
$\mathrm{H}\,(x)$	Heaviside function
k	thermal conductivity [$\mathrm{W\,m^{-1}\,K^{-1}}$]
K	permeability [$\mathrm{m^2}$]
l	cavity height [m]
L	enthalpy of fusion [$\mathrm{J\,kg^{-1}}$]
M_s	specific surface [$\mathrm{m^{-1}}$]
p	pressure [Pa]
p'	pressure without the hydrostatic contribution [Pa]
$\dot{q}$	wall heat flux [$\mathrm{W\,m^{-2}}$]
Ra	Rayleigh number [dimensionless]
S	general source term
S_e	energy equation source term [$\mathrm{W\,m^{-3}}$]
$\mathbf{S}_\mathrm{m}$	momentum equation source term [$\mathrm{kg\,m^{-2}\,s^{-2}}$]
t	time [s]
T	temperature [K]
u, $\mathbf{u}$	velocity [$\mathrm{m\,s^{-1}}$]
x, y	Cartesian coordinates [m]
β	thermal coefficient of expansion [$\mathrm{K^{-1}}$]
ε	small constant [dimensionless]
λ	porosity [dimensionless]
μ	dynamic viscosity [$\mathrm{kg\,m^{-1}\,s^{-1}}$]
ρ	density [$\mathrm{kg\,m^{-3}}$]
$\bar{\rho}$	partial density [$\mathrm{kg\,m^{-3}}$]
$\boldsymbol{\sigma}$	stress tensor [Pa]
ϕ	general scalar quantity

Subscripts and superscripts

i	initial
i	i-th component of a Cartesian vector
k	phase k
l	liquid
liq	liquidus
ref	reference value
s	solid
sol	solidus
0	reference value
I, Ia, II	denoting different forms of the momentum source term
α	constituent α

REFERENCES

1. W. D. Bennon and F. P. Incropera, A Continuum Model for Momentum, Heat and Species Transport in Binary Solid-Liquid Phase Change Systems—II. Application to Solidification in a Rectangular Cavity, *Int. J. Heat Mass Transfer*, vol. 30, pp. 2171–2187, 1987.

2. G. Amberg, Computation of Macrosegregation in an Iron-Carbon Cast, *Int. J. Heat Mass Transfer*, vol. 34, pp. 217–227, 1991.

3. W. D. Bennon and F. P. Incropera, A Continuum Model for Momentum, Heat and Species Transport in Binary Solid-Liquid Phase Change Systems—I. Model Formulation, *Int. J. Heat Mass Transfer*, vol. 30, pp. 2161–2170, 1987.

4. P. J. Prescott, F. P. Incropera, and W. D. Bennon, Modeling of Dendritic Solidification Systems: Reassessment of the Continuum Momentum Equation, *Int. J. Heat Mass Transfer*, vol. 34, pp. 2351–2359, 1991.

5. V. R. Voller and C. Prakash, A Fixed Grid Numerical Modelling Methodology for Convection-Diffusion Mushy Region Phase-Change Problems, *Int. J. Heat Mass Transfer*, vol. 30, pp. 1709–1719, 1987.

6. R. West, On the Permeability of the Two-Phase Zone During Solidification of Alloys, *Met. Trans. A*, vol. 16A, p. 693, 1985.

7. M. J. M. Krane and F. P. Incropera, A Scaling Analysis of the Unidirectional Solidification of a Binary Alloy, *Int. J. Heat Mass Transfer*, vol. 39, pp. 3567–3579, 1996.

8. J. Bear, *Dynamics of Fluids in Porous Media*. American Elsevier, New York, 1972.

9. T. S. Piwonka and M. C. Flemings, Pore Formation in Solidification, *Trans. Met. Soc. AIME*, vol. 236, pp. 1157–1165, 1966.

10. S. V. Patankar, *Numerical Heat Transfer and Fluid Flow.* Hemisphere, Washington, 1980.

11. Fluent Inc., User's Guide for Fluent/UNS & Rampant, Release 4.0. Lebanon, NH, 1996.